The Dissociation of Diacetyl: A Shock Tube and Theoretical Study

Xueliang Yang,[†] Ahren W. Jasper,[‡] John H. Kiefer,[§] and Robert S. Tranter*[,†]

Chemical Sciences and Engineering Division, Argonne National Laboratory, 9700 South Cass Avenue, Argonne, Illinois 60439, Combustion Research Facility, Sandia National Laboratory, P.O. Box 969, Livermore, California 94551, and Department of Chemical Engineering, University of Illinois at Chicago, 810 South Clinton Street, Chicago, Illinois 60607

Received: April 22, 2009; Revised Manuscript Received: May 22, 2009

The dissociation of diacetyl dilute in krypton has been studied in a shock tube using laser schlieren densitometry at 1200−1800 K and reaction pressures of 55 ± 2, 120 ± 3, and 225 ± 5 Torr. The experimentally determined rate coefficients show falloff and an ab initio/Master Equation/VRC-TST analysis was used to determine pressure-dependent rate coefficient expressions that are in good agreement with the experimental data. From the theoretical calculations $k_\infty(T) = 5.029 \times 10^{19}\ (T/298\ \mathrm{K})^{-3.40} \exp(-37665/T)\ \mathrm{s}^{-1}$ for $300 < T < 2000$ K. The laser schlieren profiles were simulated using a model for methyl recombination with appropriate additions for diacetyl. From the simulations rate coefficients were determined for $CH_3 + CH_3 = C_2H_6$ and $CH_3 + C_4H_6O_2 = CH_3CO + CH_2CO + CH_4$ ($k(T) = 2.818T^{4.00} \exp(-5737/T)\ \mathrm{cm}^3\ \mathrm{mol}^{-1}\ \mathrm{s}^{-1}$). Excellent agreement is found between the simulations and experimental profiles, and Troe type parameters have been calculated for the dissociation of diacetyl and the recombination of methyl radicals.

Introduction

The dissociation of diacetyl, 2,3-butadione, is initiated by C−C fission (1) to form two acetyl radicals which rapidly dissociate (2) to a methyl radical and CO.

$$CH_3COCOCH_3 \rightarrow CH_3CO + CH_3CO \qquad \Delta H_{r,298} = 72.9\ \mathrm{kcal/mol} \qquad (1)$$

$$CH_3CO \rightarrow CH_3CO \qquad \Delta H_{r,298} = 11.1\ \mathrm{kcal/mol} \qquad (2)$$

Thus, from each diacetyl two methyl radicals are obtained and (1) should be a clean, efficient pyrolytic source of methyl radicals at shock tube temperatures and it may be superior to some other sources we have used including ethane, acetaldehyde, and acetone. Acetone is the next easiest to dissociate of these other precursors and has a C−C bond strength that is about 10 kcal/mol higher than that of the central C−C bond in diacetyl. Consequently, diacetyl can be used for methyl generation at somewhat lower temperatures than the other precursors.

Recently, we have also investigated the dissociation of CH_3I as a source of methyl radicals[1] and developed a mechanism for methyl radical reactions that simulates both methyl recombination and ethane pyrolysis reactions very well over the temperature range 1500−2200 K. It is likely that the experimental range that (1) is observable over will overlap the CH_3I experiments providing another test for the methyl radical submechanism.

The earliest reports on the thermal decomposition of diacetyl are by Rice and Walters[2] (420−470 K, 38−458 Torr) and Walters[3] (383−436 K, 147−287 Torr) who studied the reaction in bulb experiments. Product analyses were performed, and a reaction mechanism proposed along with rate coefficients for (1). Subsequent thermal experiments were carried out in a stirred flow reactor (677−776 K, 0.6−45 Torr) by Hole and Mulcahy[4] and in a flow tube by Scherzer and Plarre[5] (822−905 K, 0.6−430 Torr). Knoll et al.[6] investigated (1) in static cells (648−690 K, 43−183 Torr). The rate coefficients for reaction 1 obtained by Knoll et al., Hole and Mulcahy, and Scherzer and Plarre are in good mutual agreement.

On the basis of product analyses from the above investigations, an investigation of acetone formation in diacetyl pyrolysis by Guenther et al.,[7] and photochemical studies by Blacet and Bell,[8,9] a reaction mechanism for the low temperature pyrolysis of diacetyl has been elucidated that satisfactorily explains the main products ketene, methane, acetone, ethane, and CO. The previous studies indicate that (1) is the sole dissociation path for diacetyl which is followed by the rapid dissociation of acetyl radicals via (2) promoting a chain reaction mechanism propagated by methyl radicals.

$$CH_3 + CH_3COCOCH_3 \rightarrow CH_4 + CH_2COCOCH_3 \qquad (3)$$

$$CH_3 + CH_3COCOCH_3 \rightarrow CH_3COCH_3 + CH_3CO \qquad (4)$$

$$CH_3 + CH_3 \rightarrow C_2H_6 \qquad \Delta H_{r,298} = -90.2\ \mathrm{kcal/mol} \qquad (5)$$

Methyl radicals attack the parent molecule via (3) and (4) and the $CH_2COCOCH_3$ radical formed in (3) readily dissociates to ketene and CH_3CO. At the low temperatures of these studies methyl recombination (5) is the main termination step.

* Corresponding author, tranter@anl.gov.
[†] Chemical Sciences and Engineering Division, Argonne National Laboratory.
[‡] Combustion Research Facility, Sandia National Laboratory.
[§] Department of Chemical Engineering, University of Illinois at Chicago.

10.1021/jp903716f CCC: $40.75
Published on Web 07/01/2009

There are no high temperature studies of diacetyl pyrolysis in the literature, and at elevated temperatures the mechanism may be complicated by reactions of H atoms generated from secondary reactions of CH_3 and dissociation of ketene. As seen from Frank et al.,[10] ketene should be stable in the temperature range of the current work.

The dissociation of acetyl radicals (2) is the primary source of CH_3 radicals in diacetyl pyrolysis. At shock tube temperatures the only experimental value for (2) is a recent estimate by Yasunaga et al.[11] which was derived from a shock tube study of acetaldehyde pyrolysis. Recommended rate coefficients for (2) also appear in compilations of kinetic data such as those of Baulch et al.[12] Reaction 2 has also been the subject of three recent theoretical investigations by Huynh et al.,[13] Senosiain et al.,[14] and Lee and Bozzelli,[15] with calculated rate coefficients covering the range 200−2500 K. Senosiain et al. estimated pressure-dependent rate coefficients that are in good agreement with the low temperature experimental results and demonstrate that dissociation of acetyl via (2) has a significantly lower barrier than other potential reactions and is the only viable route at high temperatures.

The study of diacetyl dissociation and the subsequent recombination of the resulting methyl radicals is well suited to investigation by the laser schlieren, LS, shock tube, ST, technique. The measured beam deflections are proportional to the net endothermic rate and will generate large initial positive gradients from (1) followed by strong negative gradients arising mainly from methyl recombination (5). The two processes are well-separated in time as well as sign and should be clearly seen and differentiated. A theoretical investigation of the dissociation of diacetyl has also been conducted and the results were used in a Master Equation, ME, study to investigate the pressure dependency of (1). Both initial diacetyl decomposition rates and an expanded and verified mechanism for the methyl recombination reactions and the associated chain mechanism are presented here.

Experimental Section

The LS experiments were performed in a diaphragmless shock tube, DFST, which has been fully described elsewhere.[16] The driver section of the DFST contains a fast acting valve which replaces the more traditional diaphragm. When the valve is closed by pressurizing the inside of the bellows, the driver and driven sections are separated and can be filled to the desired loading pressures. The DFST is fired by rapidly opening the valve. By variation of both the driver section pressure, P_4, and the driven section pressure, P_1, the pressure behind the incident shock wave, P_2, can be constrained to very narrow ranges, typically $<\pm 3\%$, over a wide range of temperatures.

The driven section of the shock tube has an internal diameter of 7.012 cm, and the quartz windows, through which the beam from a helium−neon laser passes for LS measurements, are located sufficiently far downstream to allow the shock wave to be fully developed after firing the DFST. A set of six pressure transducers evenly spaced along the side of the driven section are centered around the LS windows, and incident shock wave velocities were obtained by interpolation of the five intervals calculated from the measured times taken for the shock wave to arrive at successive pressure transducers. From these velocities and the loading conditions, the temperature and pressure behind the incident shock wave are calculated assuming frozen conditions. The uncertainty in velocity is estimated as 0.2%, corresponding to a temperature error of less than 0.5%, here amounting to the order of 10−15 K.

The LS diagnostics and technique have been thoroughly described previously.[17,18] The molar refractivity of Kr = 6.367,[19] while that of diacetyl, 20.99, was calculated from its refractive index (1.394) and molar density (0.981 g/cm^3). The usual assumption is made that for the dilute reagent mixtures used in this work the mixture molar refractivity does not vary significantly with extent of reaction.

Mixtures containing 1% and 2% diacetyl dilute in krypton were prepared manometrically in a 50 L glass vessel that had been evacuated to $<10^{-3}$ Torr. Krypton (AGA 99.999%), was used as supplied. Diacetyl (Aldrich Chemical Co., 99%) was degassed by repeated freeze−pump−thaw cycles with liquid nitrogen. Reagent mixtures were allowed to homogenize for several hours before use. The uncertainty in the mixture composition is <0.1%.

Theory

The capture (high pressure limit) kinetics for the self-recombination of CH_3CO were computed using direct variable reaction coordinate transition state theory[20−22] (VRC-TST), as implemented in the computer code VaReCoF.[23] The interaction potential energy surface was evaluated on-the-fly using the CASPT2 method and a two-electron, two-orbital active space. Dividing surfaces were constructed by placing pivot points at the center of mass of the fragments, at the reactive C atom, or displaced from the reactive C atom in the direction of the radical orbital by 0.3 or 0.5 Å. For each pivot point type, pivot point separations from ∼3 to 10 Å were included in the microcanonical variational optimizations.

In the VRC-TST calculations, the CH_3CO fragments were kept fixed at their B3LYP/6-311++G(d,p) equilibrium geometries. Bimolecular H abstraction channels give rise to shallow wells in the fixed-fragment interaction potential energy surface at fragment separations of ∼3 Å. This region of the potential energy surface corresponds to the dynamical bottlenecks for association at moderate and high temperatures. When the kinetics for dividing surfaces with fragment separations greater than 5 Å were evaluated, the infinite potential method[22] was used to isolate the deep attractive well associated with the capture process from features in the potential energy surface associated with the abstraction channels. For fragment distances greater than ∼5 Å, the interaction potential is controlled by long-range forces, which are only weakly dependent on fragment orientation. The full range of fragment orientations was included when evaluating the kinetics for dividing surfaces in this outer region of the interaction potential. The overall association kinetics were obtained using a two-transition-state model[24,25] to combine the calculated kinetics for the inner and outer regions.

The basis set dependence of the computed rate coefficients was considered for the cc-pVDZ and aug-cc-pVDZ basis sets[26,27] and for the one-dimensional basis set correction potential (BSCP) scheme for C−C bond-forming reactions developed elsewhere.[28] Both the BSCP and the aug-cc-pVDZ basis sets predict faster capture rates than the cc-pVDZ basis set by 30−60% for 300−2000 K. The rates calculated using the BSCP and aug-cc-pVDZ methods are in fair agreement with one another, differing by ∼10%, and the BSCP scheme is used exclusively throughout the rest of this article.

A potential energy diagram for diacetyl decomposition was computed at the QCISD(T)/CBS//B3LYP/6-311++G(d,p) level of theory, where the complete basis set (CBS) limit[29] was estimated from aug-cc-pVDZ and aug-cc-pVTZ calculations. The results are summarized in Table 1. The calculated values

TABLE 1: Selected 0 and 298 K Stationary Point Energies for Diacetyl Decomposition (kcal/mol)

stationary point	exptl[a]	calcd[b]
2 CH_3CO	[0.0]	0.00 [0.00]
$CH_3COCOCH_3$	[−72.4, −72.0 ± 2.8[c]]	−72.56 [−73.58]
$CH_3CHO + CH_2CO$	[−46.5]	−46.40 [−46.71]
$CH_3COH + CH_2CO$		4.02
$CH_2CHO + CH_3CO$		6.85

[a] Experimental values at 298 K from reference 30. [b] QCISD-(T)/CBS//B3LYP/6-311++G(d,p) values at 0 K and [298 K]. [c] Reference 31.

are in good agreement with available experimental[30,31] channel energies at 298 K. The quantum chemistry calculations were carried out using Gaussian03[32] and Molpro 2006.[33]

There are several bimolecular products that may be formed upon breaking the central C−C bond of diacetyl. Three dissociation processes involve a concerted H atom transfer as the C−C bond is broken. As seen in Table 1 the $CH_3CHO + CH_2CO$ products are the most energetically favorable, but no low-energy bond breaking saddle point to these products could be found. Decomposition to the $CH_3COH + CH_2CO$ and $CH_2CHO + CH_3CO$ products also likely proceeds via tight transition states with correspondingly large barriers. We note that the Q_1 diagnostics[34] for these saddle points are ∼0.04, which may indicate that a multireference approach is required to more accurately characterize these processes.[35]

Diacetyl may also dissociate without a reverse barrier via a loose transition state to give two acetyl radicals (1). The dissociation kinetics may be sensitive to the bond energy of the breaking bond, and we tested the sensitivity of the computed 0 K bond energy (E_0 = 72.56 kcal/mol) to several aspects of the calculation. Extrapolating from the aug-cc-pVTZ and aug-cc-pVQZ basis sets has a minor effect on the QCISD(T)/CBS//B3LYP/6-311++G(d,p) bond energy, giving 72.60 kcal/mol. With MP2/6-311++G(d,p) geometries, the computed QCISD(T)/CBS//B3LYP/6-311++G(d,p) bond energy is 72.74 kcal/mol. The CCSD(T)/CBS//B3LYP/6-311++G(d,p) method predicts a bond energy of 73.08 kcal/mol. All four dual level methods predict values within the estimated 2σ (∼95% confidence limit) uncertainty of the QCISD(T)/CBS//B3LYP/6-311++G(d,p) method (∼4 kcal/mol).

The lowest-energy pathway for diacetyl decomposition is the formation of two acetyl radicals, and this channel is considered exclusively in the master equation calculations. Other channels may contribute to the overall dissociation dynamics, but we expect these contributions to be negligible. In particular, although the channel energy for $CH_2CHO + CH_3CO$ is similar to that of $2CH_3CO$ and the reverse barrier is low, the $CH_2CHO + CH_3CO$ products are formed via a tight transition state, which is likely strongly disfavored relative to the lower-energy $2CH_3CO$ products formed via a loose, barrierless transition state. The formation of two acetyl radicals as the exclusive products of diacetyl decomposition is in agreement with the experimental studies discussed above.

Two-dimensional ME calculations[36] for $CH_3COCOCH_3 \Leftrightarrow 2CH_3CO$ were carried out using the VRC-TST capture kinetics, the B3LYP/6-311++G(d,p) frequencies and geometries, and the VariFlex computer code.[37] The exponential down model was used to treat collisional energy transfer, where the average

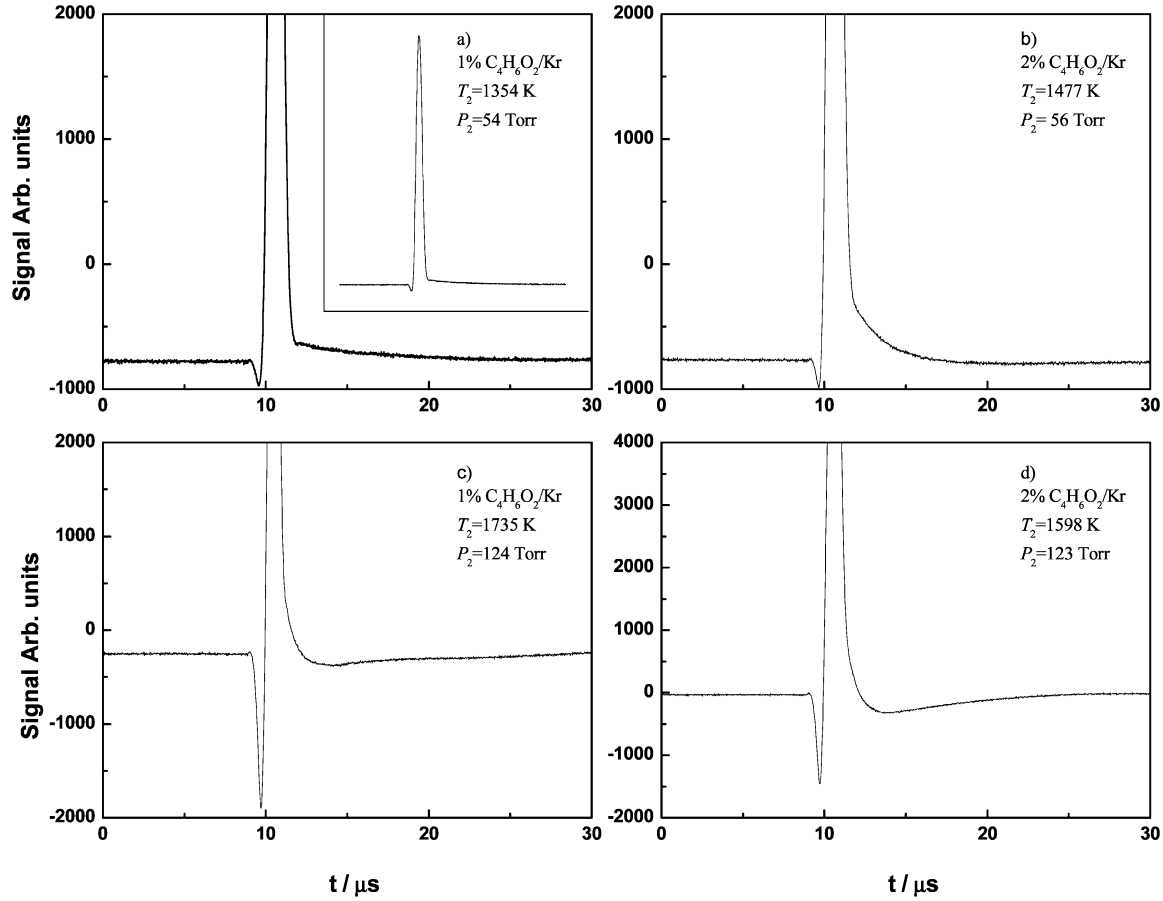

Figure 1. Example raw signals from LS experiments with 1% and 2% diacetyl dilute in krypton. The figures have been expanded vertically to show the curvature due to reaction more clearly. The inset figure in (a) shows the complete signal.

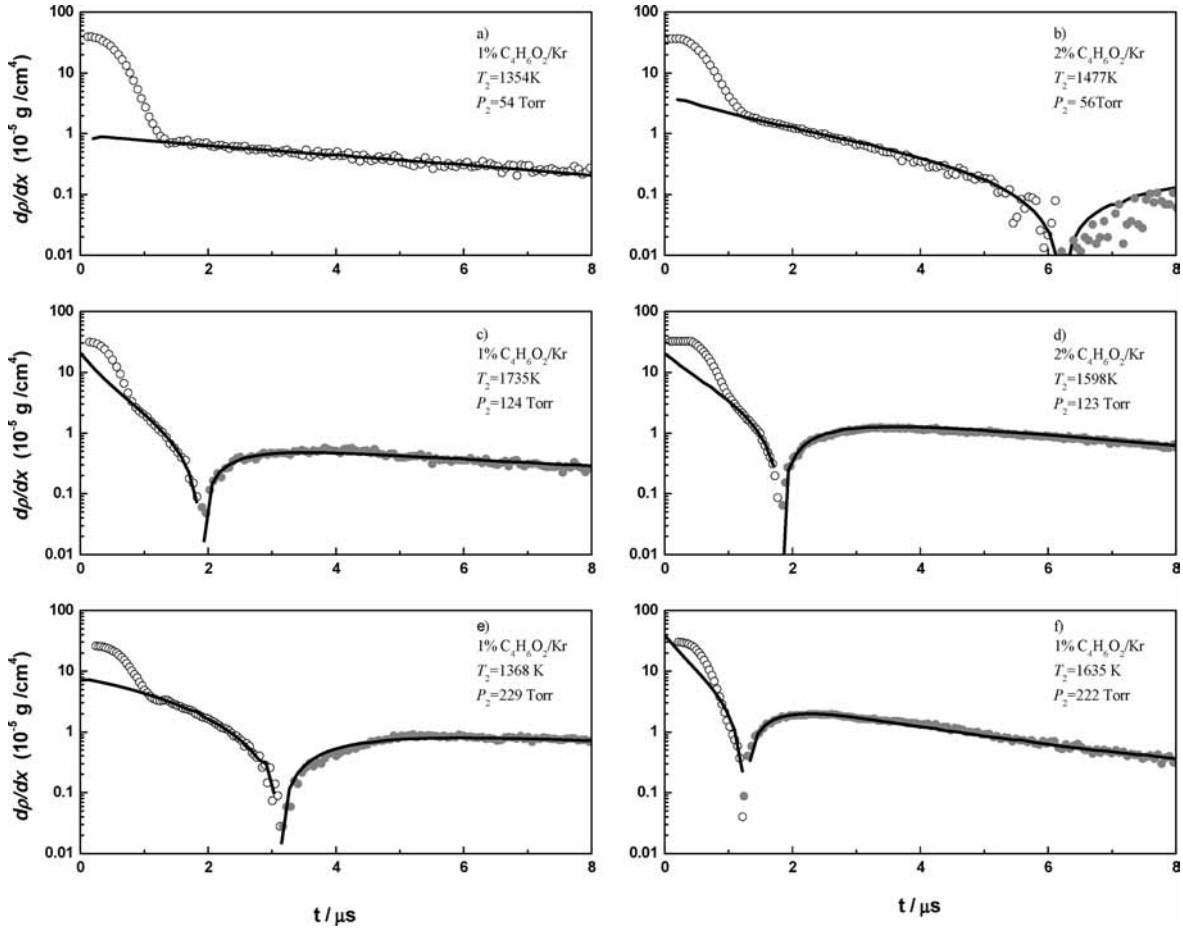

Figure 2. Example semilog density gradient plots derived from the raw LS signals the experiments with 1% and 2% diacetyl dilute in krypton. Absolute values are plotted, and open symbols represent positive values and closed symbols represent negative values. The symbols represent experimental data, and the lines are results of simulations using the model in Table 1 with optimum values for R_1, R_2, and R_3. Parts a−d correspond to the plots in Figure 1a−d.

downward energy transfer, α, was parametrized as a function of temperature.

$$\alpha(T) = \alpha_{300}(T/300\ \mathrm{K})^n$$

The dissociation energy (E_0) and energy transfer parameters (α_{300} and n) were taken as fitting parameters and will be discussed below.

Results and Discussion

A total of 88 ST/LS experiments have been performed over the temperature range $1200 < T_2 < 1800$ K and $P_2 = 55 \pm 2$ Torr, $P_2 = 120 \pm 3$ Torr, and $P_2 = 225 \pm 5$ Torr. The conditions and results for each experiment are tabulated in the Supporting Information. For both the 55 and 120 Torr experiments reaction mixtures of 1% and 2% diacetyl dilute in krypton were used. Only the 1% mixture was used in the 225 Torr experiments as the higher concentration mixture introduced instabilities in the LS signal which are presumably due to excessive heat release from the strongly exothermic reaction of methyl recombination. Examples of the raw laser schlieren profiles covering the complete experimental range are shown in Figure 1. All of the LS profiles have several common features. The large, positive spike and the preceding negative spike are due to diffraction and refraction of the laser beam as the shock front passes through it.[38] The remaining signal to the right of the large spike is due to chemical reaction. In the lower pressure and lower temperature experiments, e.g., Figure 1a, there is a sharp change in the signal whereas in the experiments where the initial dissociation is more rapid this break in the signal can be harder to identify; see for example Figure 1c. However, the break is usually easy to identify on semilog plots like those of parts c and d of Figure 2. With the exception of the low temperature 55 Torr experiments, all the LS profiles have minima that dip below the signal which precedes arrival of the shock wave, used to define the baseline in each experiment, and then recover to the baseline. These minima in LS signals are characteristic of net exothermic processes and provide valuable targets for mechanism development and, in favorable cases, obtaining kinetic data for secondary reactions.

Semilog plots of the density gradient profiles derived from the raw data are shown Figure 2 where parts a−d of Figure 2 correspond to the LS profiles in parts a−d of Figure 1. The first few steeply falling points in each figure are due to the end portion of the shock front/laser beam interaction described above which unfortunately masks the location of t_0, the time origin at the onset of reaction. Consequently, t_0 is located by a well-established method[38] and typically is determined to within 0.1−0.2 μs. The time origin corrections are largest for the lowest pressure experiments where there is greater curvature in the shock front.

Dissociation of Diacetyl. At the time origin the only reaction contributing to the density gradient is the initial dissociation of

diacetyl, and by extrapolating the density gradient profiles back to t_0 accurate estimates for the rate coefficient, k_1, are obtained. For experiments where the initial rates of reaction are fairly small, e.g., parts a and b of Figure 2, this extrapolation is quite accurate. However, as the rate increases, the extrapolation becomes somewhat less certain and k_1 is best determined through simulation of the whole density gradient profile, discussed later, using a well-established iterative procedure. The initial estimates for k_1 do not typically change by more than 10−20%.

In a number of the 55 Torr experiments the optimized simulation results run close to the experimental data but parallel it on the underside and reasonable modifications to rate coefficients and thermochemical parameters only serve to worsen the agreement. Typically, this occurs not because of deficiencies in the mechanism but it is due instead either to error in the location of t_0 or to incubation. In diacetyl/Kr mixtures relaxation is very fast and we have been unable to resolve it even at very low temperatures and pressures. Our best estimates of incubation times at 55 Torr are 0.2−0.3 μs, close to the error in t_0. Consequently, for experiments such as those shown in parts a and b of Figure 2, the start of simulation has been delayed by 0.2 μs to account for these effects. The effect of this shift on the value of the density gradient at t_0 and hence k_1 is negligible.

The first-order rate coefficients determined from the 55, 120, and 225 Torr LS experiments are presented in Figure 3 where they are also compared to the theoretical results of the ME/VRC-TST work. The experimental decomposition rate coefficients are in the falloff region at the pressures of interest (55−225 Torr Kr), and the results of the theoretical calculations are therefore sensitive to the bond energy and to the energy transfer parameters used in the ME calculations. With the calculated value of $E_0 = 72.6$ kcal/mol, the experimental data were well fit using a temperature-independent form for the energy transfer parameter ($\alpha_{300} = 1000$ cm^{-1} and $n = 0$), dotted lines in Figure 3. However, very good agreement with the experimental data is obtained using $E_0 = 70.0$ kcal/mol and a temperature-dependent form for the energy transfer parameter ($\alpha_{300} = 210$ cm^{-1}, and $n = 0.7$), solid lines Figure 3. Such an adjustment to the bond energy is justified as it is within the uncertainties of the experimental and theoretical bond energies. Furthermore, α is often found to have a positive temperature dependence, with $n = 0.5-1$. The theoretical calculations obtained using $E_0 = 70.0$ kcal/mol are therefore preferred, and these results were fit to modified Arrhenius forms over the range 1200−1800 K and k_∞ was fit over the range 300−2000 K.

$$k_{55\text{Torr}}(T) = 7.7 \times 10^{31}(T/298\text{ K})^{-19.3} \times \exp(-46140\text{ K}/T)\text{ s}^{-1}$$

$$k_{120\text{Torr}}(T) = 1.42 \times 10^{33}(T/298\text{ K})^{-20.0} \times \exp(-47973\text{ K}/T)\text{ s}^{-1}$$

$$k_{220\text{Torr}}(T) = 7.36 \times 10^{33}(T/298\text{ K})^{-20.3} \times \exp(-49099\text{ K}/T)\text{ s}^{-1}$$

$$k_\infty(T) = 5.02 \times 10^{19}(T/298\text{ K})^{-3.40} \times \exp(-37665\text{ K}/T)\text{ s}^{-1}$$

Clearly, the agreement between the results of the LS experiments and the theoretical calculations is very good.

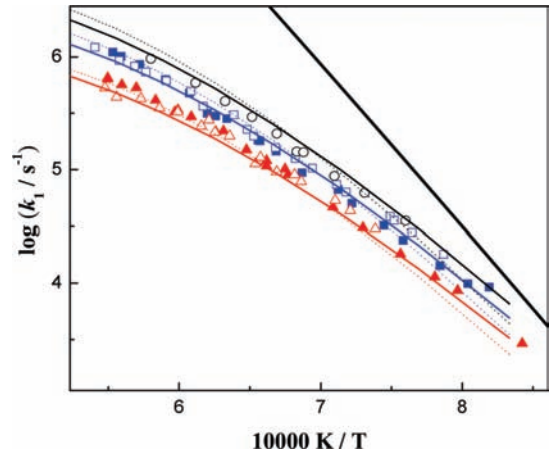

Figure 3. Arrhenius plot of first order-experimental rate coefficients for reaction 1 at different pressures: 1% $C_4H_6O_2$/Kr at 225 Torr (black open circles), 120 Torr (blue open box), and 55 Torr (red open triangle) and 2% $C_4H_6O_2$/Kr at 120 Torr (solid blue box) and 55 Torr (solid red triangle). Solid lines represent the preferred master equation calculations with $E_0 = 70$ kcal/mol, $\alpha_{300} = 210$ cm^{-1}, and $n = 0.7$ where $\alpha(T) = \alpha_{300}(T/300\text{ K})^n$: k_∞ (bold black solid line), 220 Torr (black solid line), 120 Torr (blue solid line), and 55 Torr (red solid line). Dotted lines represent master equation calculations with $E_0 = 72.6$ kcal/mol and $\alpha = 1000$ cm^{-1}: 220 Torr (black dotted line), 120 Torr (blue dotted line), and 55 Torr (red dotted line).

Furthermore, the high pressure limit rate coefficient has also been compared with the low temperature experimental results of Scherzer and Plarre,[5] Knoll et al.,[6] and Hole et al.[4] in Figure 4, and here the agreement is also good. To aid in modeling, the present theoretical results were also fit to Troe forms[39,40] given below

$$k_\infty(T) = 5.02 \times 10^{19}T^{-3.40}\exp(-74840\text{ cal}/(\text{mol}/RT))\text{ s}^{-1}$$

$$k_0(T) = 1.63 \times 10^{48}T^{-9.17} \times \exp(-51830\text{ cal}/(\text{mol}/RT))\text{ cm}^3\text{ mol}^{-1}\text{ s}^{-1}$$

$$F_{\text{cent}} = (1 - 0.520)\exp(-T/3074\text{ K}) + 0.520\exp(-T/496\text{ K}) + \exp(-4100\text{ K}/T)$$

for 1200−1800 K and 55−220 Torr.

Although the focus of the present work is the dissociation of diacetyl, we have also briefly compared the calculated association rate coefficient, the reverse of (1), with available experimental measurements. At room temperature, the VRC-TST capture rate coefficient (3.2×10^{-11} cm^3 molecule^{-1} s^{-1}) is within the range of experimental results[41−44] ($(1.4-3.9) \times 10^{-11}$ cm^3 molecule^{-1} s^{-1}), as shown in Figure 5. The present results predict a negative temperature dependence in agreement with the experimental results for 200−350 K in ref 44, although the experimental temperature dependence is somewhat stronger. The calculated rate coefficients are independent of pressure (down to at least 1 Torr) for temperatures below ~400 K. Note that we have not included the effect of abstraction reactions, which likely contribute to the overall bimolecular reaction rate at elevated temperatures. The VRC-TST $CH_3CO + CH_3CO$ capture rate was fit to the modified Arrhenius form: 2.95×10^{-11} $(T/298\text{ K})^{-0.908}\exp(-57.5\text{ K}/T)$ cm^3 molecule^{-1} s^{-1} for 300−1000 K.

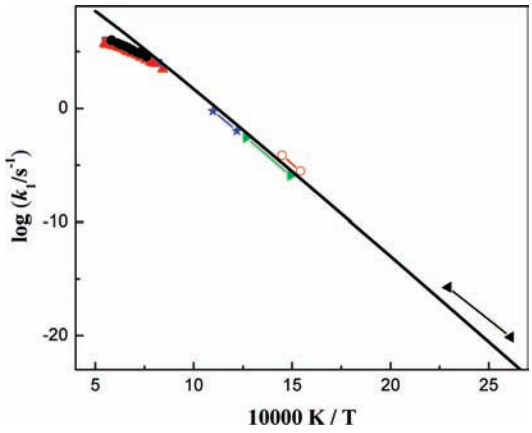

Figure 4. Comparison of the theoretical k_∞ (—) from the current work with literature data for reaction 1. Points are the experimental values from the current work: $C_4H_6O_2$/Kr at 225 Torr (solid black circle), 120 Torr (solid blue square), and 55 Torr (solid red triangle). The literature data are (solid blue star) Sherzer and Plarre,[5] (open red circle) Knoll et al.[6] (solid green trangle, right) Hole and Mulcahy,[4] and (solid black triangle, left) Walters.[3]

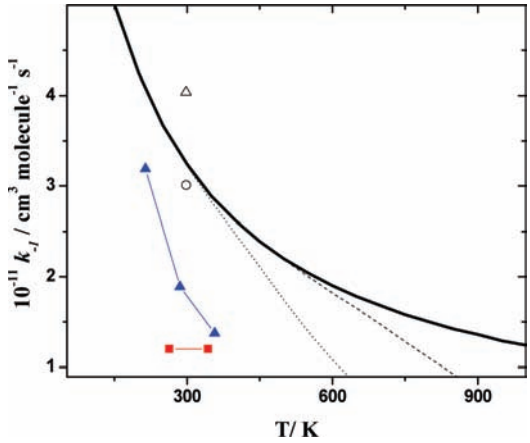

Figure 5. Calculated association rate coefficients for acetyl radicals at 1 Torr (dotted), 100 Torr (dashed), and in the high-pressure limit (solid). Also shown are the experimental measurements of Parkes[41] (black open circles), Timonen et al.[42] (black open triangles), Anastasi and Maw[43] (solid red squares), and Maricq and Szente[44] (solid blue triangles).

Modeling

In Figure 2 simulations of the experimental profiles are shown. These were obtained using a computer code designed to model reactive flows behind shock waves using a methodology similar to that outlined by Gardiner.[45] The program accounts for temperature changes as the reaction progresses, and reverse reactions are included for all reactions through the equilibrium constants and detailed balance. The model used is presented in Table 2 and essentially consists of two parts: a portion that describes the chemistry associated with diacetyl, R_1 and $R_{29}-R_{36}$, and a submechanism that describes the reactions related to methyl radicals. The later part has been taken directly from a recent LS study on the dissociation of methyl iodide[1] at similar pressures to the current work and 1500−2200 K. The notation R_x refers to reaction numbers in Table 2.

Analysis of the simulation results based on the mechanism presented in Table 2 indicates the following: R_1 is the sole reaction at t_0 but dissociation of acetyl radicals to form CH_3 and CO, R_{29}, is so rapid that even for the lowest temperature experiments it starts to make a small positive contribution to the total density gradient at around 1 μs. This is offset to some extent by R_2 the exothermic recombination of methyl radicals to form ethane which starts as soon as the methyl radical pool develops. Similar to the observations of Yang et al.[1] the location and depth of the minima in the density gradient profiles are sensitive to the rate of R_2. In fact for relatively low reaction temperatures the density gradient profiles are very well described by a three reaction mechanism consisting only of R_1, R_2, and R_{29}, as shown in Figure 6a (1398 K, 229 Torr) where the results from the full model and three reaction model are virtually indistinguishable.

The dashed blue line in parts b and c of Figure 6 shows the result of simulating a high temperature experiment (1694 K, 120 Torr) with the simple three reaction model. While the simulation could be considered adequate and the simulation hits the first few points of density gradient due to reaction, there are several important deficiencies. First of all, the location of the cusp where the profile crosses from net positive to net negative density gradient is missed, although the deviation is within the uncertainty in the location of t_0. Second, the curvature prior to the cusp is underpredicted. Finally, the late curvature is incorrect. Simply modifying t_0 within its error limits may improve the fit to one of these deficiencies, but it will not correct all of them. With the full model the cusp and the curvature are correctly predicted, and this improvement is due to a sequence of reactions involving ketene that contribute to the density gradients at higher temperatures.

The above sequence of reactions is initiated by R_{30} and R_{31}, the attack of H atoms and methyl radicals on diacetyl, respectively. R_{31} is a combination of reactions 3 and 4 from the introduction. R_{30} and R_{31} would generate the same radical product as (3), $CH_2COCOCH_3$, and this is assumed to readily dissociate to the products CH_2CO and CH_3CO. Although R_{30} and R_{31} do not contribute significantly to the density gradient due to their small heats of reaction, ($\Delta H_{r,298K}$ = 12.2 and 11.4 kcal/mol, respectively) they do affect the profile by generating methyl radicals and ketene. Under the conditions of the current work ketene does not dissociate by R_{32} however it is removed by reaction with CH_3 radicals via R_{34} to generate C_2H_5 and CO. At high temperatures R_{34} makes a maximum contribution to the total density gradient at about 1 μs whereas at low temperatures R_{34} is insignificant until at least 5 μs when it starts to make negative contributions that quickly become quite important. The C_2H_5 radicals subsequently decompose via R_{-6} ($H_{r-6,298K}$ = 36 kcal/mol) which is responsible for a significant positive contribution to the density gradient at late times. Ketene is also removed by reaction with H-atoms to form CH_3 and CO by R_{33} although this is only a minor route at high temperatures and negligible at low temperatures. The effect of doubling k_{31} is shown by the red dashed line in Figures 6b and 6c, and while the effect is apparently small it is nonetheless significant.

At high temperatures the reactions of methylene also become important. $^3CH_2$ and $^1CH_2$ are formed by recombination of methyl radicals via R_{-16} ($H_{r,298}$ = 5.5 kcal/mol) and R_{-23} ($H_{r,298}$ = 14.5 kcal/mol). $^3CH_2$ reacts exothermically with CH_3, R_{15}, and is one of the main sources of late negative density gradients. $^1CH_2$ is rapidly quenched to $^3CH_2$, R_{25} and the remaining reactions of $^1CH_2$ are only minor contributors to the total density gradient. These sequences of predominantly bimolecular reactions are more significant at high temperatures and of course are somewhat sensitive to the initial concentration of diacetyl and the reaction pressure. The remaining reactions in Table 2 make either small or no contributions to the observed density gradients.

TABLE 2: Reaction Mechanism and Arrhenius Parameters for Diacetyl Pyrolysis[a]

	reaction	log A	n	E_a	ref	$\Delta_f H_{298}$
R_1	*$CH_3COCOCH_3 + M = CH_3CO + CH_3CO + M$*	*40.700*	*−6.62*	*58.9*	*this work*	*72.9*
R_2	*$C_2H_6 + M = CH_3 + CH_3 + M$*	*18.200*	*0.00*	*70.0*	*this work*	*90.2*
R_3	$C_2H_6 + H = C_2H_5 + H_2$	2.740	3.50	5.2	*b*	−3.5
R_4	$C_2H_6 + CH_3 = C_2H_5 + CH_4$	−0.261	4.00	8.3	*b*	−4.3
R_5	$CH_3 + CH_3 = C_2H_5 + H$	13.732	0.00	16.1	*b*	10.6
R_6	$C_2H_4 + H = C_2H_5$	40.870	−8.81	11.6	*b*	−36.0
R_7	$C_2H_4 + H = C_2H_3 + H_2$	7.703	1.93	13.0	*b*	6.2
R_8	$CH_4 + M = CH_3 + H + M$	47.219	−8.00	121.5	*b*	105.0
R_9	$C_2H_4 + M = C_2H_2 + H_2 + M$	17.310	0.00	78.3	*b*	42.0
R_{10}	$C_2H_4 + M = C_2H_3 + H + M$	17.413	0.00	96.6	*b*	110.4
R_{11}	$C_2H_5 + H = C_2H_4 + H_2$	12.300	0.00	0.0	*b*	−68.2
R_{12}	$C_2H_2 + H = C_2H_3$	30.248	−5.98	6.0	*b*	−35.8
R_{13}	$C_2H_3 + H = C_2H_2 + H_2$	13.600	0.00	0.0	*b*	−68.4
R_{14}	$CH_4 + H = CH_3 + H_2$	5.7780	2.50	9.7	*b*	0.8
R_{15}	$CH_2(T) + CH_3 = C_2H_4 + H$	15.070	−0.34	0.2	*b*	−63.9
R_{16}	$CH_4 + CH_2(T) = CH_3 + CH_3$	6.390	2.00	8.3	*b*	−5.5
R_{17}	$CH_2(S) + H_2 = H + CH_3$	13.800	−0.00	0.0	*b*	−15.3
R_{18}	$CH_3 + M = CH_2(T) + H + M$	16.000	0.00	90.6	*b*	110.5
R_{19}	$C_3H_8 + M = CH_3 + C_2H_5 + M$	18.892	0.00	64.9	*b*	88.7
R_{20}	$CH_3 + C_2H_5 = C_2H_4 + CH_4$	11.950	0.00	0.0	*b*	−69.0
R_{21}	$H + H + M = H_2 + M$	18.000	−1.00	0.0	*b*	−104.2
R_{22}	$C_2H_6 = H + C_2H_5$	42.519	−8.07	110.4	*b*	100.8
R_{23}	$CH_2(S) + CH_4 = CH_3 + CH_3$	13.204	0.00	−0.6	*b*	−14.5
R_{24}	$CH_2(S) + CH_3 = C_2H_4 + H$	13.079	0.00	−0.6	*b*	−72.8
R_{25}	$CH_2(S) + M = CH_2(T) + M$	12.950	0.00	0.6	*b*	−9.0
R_{26}	$CH_2(S) + C_2H_6 = CH_3 + C_2H_5$	13.600	0.00	−0.6	*b*	−18.8
R_{27}	$CH_2(T) + CH_2(T) = C_2H_2 + H_2$	13.500	0.00	−0.0	*b*	−132.5
R_{28}	$CH_2(T) + H_2 = H + CH_3$	5.700	2.00	7.2	*b*	−6.3
R_{29}	$CH_3CO = CH_3 + CO$	16.500	−2.09	15.2	*b*	11.1
R_{30}	$CH_3COCOCH_3+H=CH_3CO+ CH_2CO +H_2$	7.962	2.00	5.0	estimated	12.2
R_{31}	*$CH_3COCOCH_3 + CH_3 = CH_3CO + CH_2CO + CH_4$*	*0.450*	*4.00*	*7.9*	*this work*	*11.4*
R_{32}	$CH_2CO = CH_2(T) + CO$	15.361	0.00	57.6	10	78.1
R_{33}	$CH_2CO + H = CH_3 + CO$	8.900	1.45	2.8	14	−32.4
R_{34}	$CH_2CO + CH_3 = C_2H_5 + CO$	12.699	0.00	0.0	49	−21.8
R_{35}	$CH_3COCH_3 = CH_3 + CH_3CO$	16.400	0.00	81.7	47	83.9
R_{36}	$CH_3 + CH_3CO = C_2H_6 + CO$	13.300	0.00	0.0	50	−79.1

[a] Units: kcal/mol, mole, cm^3, s. The values shown for R_1, R_2, and R_{31}, highlighted in italics, have been optimized for 120 Torr. $k = AT^n \exp^{(-Ea/RT)}$. [b] Reaction appears in mechanism in ref 1.

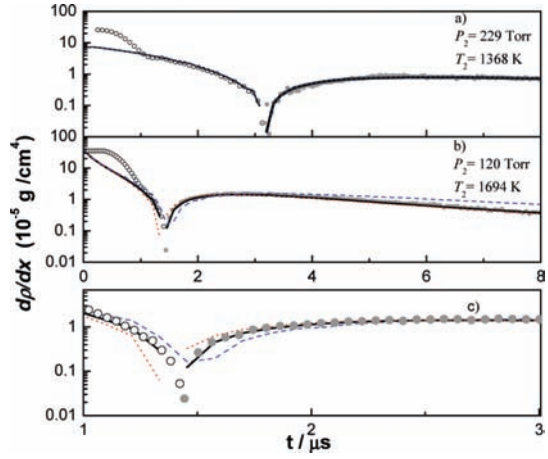

Figure 6. Comparison of the simulation with the full model and three reaction model (see text for details) and the sensitivity to k_{31}. Absolute values are plotted. (open circle) and (solid circle) represent positive and negative experimental density gradients, respectively. (solid black line) represents simulations with the full model and optimized rate coefficients. (red dotted line) represents full model with $2k_{31}$. (blue dashed line) simulation with the three reaction model. Part c is a blow up of part b between 1 and 3 μs to show more clearly the effect of varying k_{31}.

There appears to be no literature data for R_{30}, and for R_{31} the data are few and limited to low temperatures.[4−7,46] Consequently, k_{30} was estimated by analogy with an estimate of H + $CH_3COCH_3 = H_2 + CH_3COCH_2$ from a shock tube on acetone pyrolysis and oxidation.[47] To account somewhat for differences in bond strengths and internal rotors between acetone and diacetyl that should give larger rate coefficients with diacetyl, the initial estimate of k_{30} was increased by a factor of 4. Initial, simulations with various values of k_{30} had only small effects on the quality of the simulations, whereas they showed considerably more sensitivity to the value of k_{31}. Consequently, k_{30} was fixed and k_{31} was adjusted for each experiment yielding the expression given in Table 2. In the final modeling, the rate coefficients for R_1, R_2, and R_{31} were varied to optimize the fit to each experimental profile with all other rate coefficients being fixed, and where appropriate rate coefficient expressions were calculated from stated Troe parameters for each reaction pressure.[1]

The results of optimized simulations are shown in Figure 2 by the solid lines. In these figures absolute values are plotted and the transition from net positive to net negative density gradients is indicated by the sharp cusps in Figure 2b−f. The simulations clearly locate this crossing point accurately over a wide range of conditions and initial reagent concentration. Furthermore the simulations also capture the overall shapes of the density gradient profiles very well. As part of the modeling effort, the rates of the reactions identified above as contributing to the overall density gradient were varied within the error limits of their literature values and the effect on k_1 and k_2 examined. The maximum change in the optimum values of k_1 and k_2 was

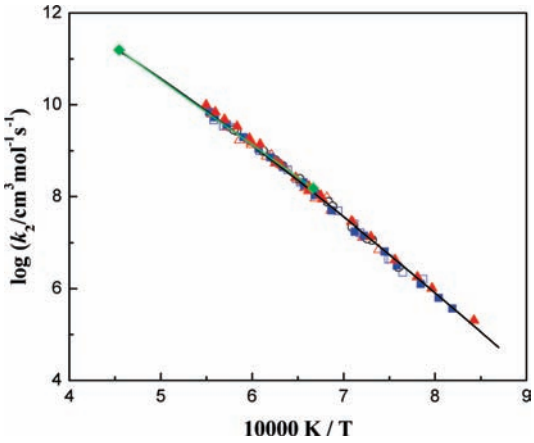

Figure 7. Arrhenius plot of the optimized second-order rate coefficients for reaction 2 from this work and ref 1: 1% $C_4H_6O_2$/Kr at 225 Torr (black open circle), 120 Torr (blue open box), and 55 Torr (red open triangle) and 2% $C_4H_6O_2$/Kr at 120 Torr (solid blue box) and 55 Torr (solid red triangle). Green diamonds and green line represent k_2 from ref 1. The black solid line is fit to all the data from the current work and ref 1 which can be expressed by $k = 10^{22.71}T^{-4.05}$ exp(−21880/*RT*).

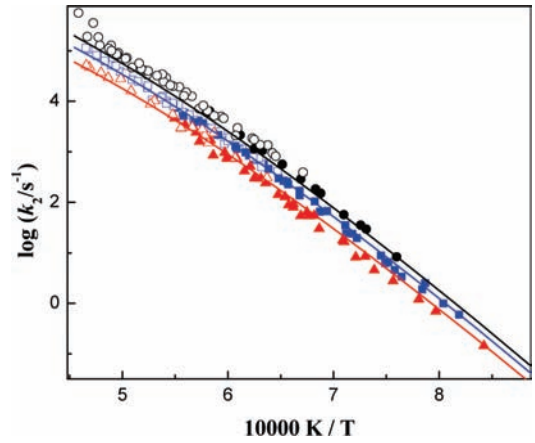

Figure 8. Comparison of experimental rate coefficients for reaction 2 from this work and CH_3I decomposition experiments of Yang et al.[1] The symbols represent the experimental values: $C_4H_6O_2$/Kr at 225 Torr (solid black circles) and 120 Torr (solid blue squares) and CH_3I/Kr at 280 Torr (black open circles), 146 Torr (blue open squares), and 55 Torr (red open triangles). The lines are the results of the ME calculations empirically adjusted to fit the experimental data: 60 Torr (red line), 130 Torr (blue line), and 250 Torr (black line).

<5% with the greatest effect being found in the high temperature experiments with 2% diacetyl, which are most sensitive to the secondary reactions.

k_2 was optimized for each experiment, and the bimolecular rate coefficients are plotted in Figure 7 along with those determined at similar pressures in the methyl iodide dissociation studies of Yang et al.[1] The two sets of data are in very good agreement with the largest deviation being <10% in the region where the experiments overlap and thus the range that k_2 has been determined by laser schlieren experiments has been considerably extended and now spans 1200−2200 K.

Previous ME calculations by Kiefer et al.[48] were optimized for temperatures above 1500 K and are in excellent agreement with the experimental results of Yang et al. and the current work for these temperatures. However, below 1500 K the ME calculations tend to overpredict the experimental data. New ME calculations for (2) were carried out in the present work using theoretical methods very similar to those of ref 48. The results of the two sets of calculations are in quantitative agreement with one another when the energy transfer parameters (α_{300} = 120 cm^{-1} and n = 0.9) and bond energy (E_0 = 87.9 kcal/mol) of Kiefer at al.[48] were used. These energy transfer parameters were readjusted to better fit the present set of expanded experimental data over 1200−2200 K. The optimized theoretical rate coefficients with α_{300} = 45 cm^{-1} and n = 1.4 are shown in Figure 8, and these results were fit to modified Arrhenius forms over the range 1000−2200 K.

$$k_{2,60\text{Torr}}(T) = 3.35 \times 10^{27}(T/298\text{ K})^{-13.7} \times \exp(-55006\text{ K}/T)\text{ s}^{-1}$$

$$k_{2,130\text{Torr}}(T) = 4.81 \times 10^{27}(T/298\text{ K})^{-13.5} \times \exp(-55193\text{ K}/T)\text{ s}^{-1}$$

$$k_{2,250\text{Torr}}(T) = 5.74 \times 10^{27}(T/298\text{ K})^{-13.3} \times \exp(-55319\text{ K}/T)\text{ s}^{-1}$$

For 1200−1500 K and 60−250 Torr, the present set of updated theoretical rate coefficients for ethane decomposition is ∼30% lower than the theoretical fits reported in ref 48. Above 2000 K, the two theoretical results are in good agreement with one another. The Troe forms provided in ref 48 for (2) have been adapted to fit the results of the present theoretical calculations

$$k_{2,\infty}(T) = 8.03 \times 10^{28}T^{-3.52} \times \exp(-95346\text{ cal/(mol/RT)})\text{ s}^{-1}$$

$$k_{2,0}(T) = 2.80 \times 10^{72}T^{-15.1} \times \exp(-107745\text{ cal/(mol/RT)})\text{ cm}^3\text{ mol}^{-1}\text{ s}^{-1}$$

$$F_{\text{cent}} = (1 - 0.557)\exp(-T/293\text{ K}) + 0.557 \times \exp(-T/637\text{ K}) + \exp(-3600\text{ K}/T)$$

for 1200−2200 K and 60−250 Torr.

Conclusions

The dissociation of diacetyl has been studied at high temperatures and low pressures in a shock tube significantly extending the range of experimental conditions. The initial dissociation is in the fall off range, and a theoretical model has been constructed that correctly predicts the pressure dependence and provides a good fit to the experimental results using reasonable estimates of E_0 and the downward energy transfer parameter.

A mechanism for the high temperature dissociation of diacetyl has also been developed, and excellent agreement between the model and experimental LS profiles is obtained. At low temperatures the contributions from potentially interfering reactions R_{31} and R_{32} are very minor as is any contribution from R_{32}, ketene dissociation. However, at the higher temperatures of this work, these reactions while minor are not negligible. Consequently, diacetyl pyrolysis can be considered as quite a clean, efficient source of methyl radicals below around 1500 K, particularly when low dilutions of reagent are employed.

Methyl recombination has now been studied by LS from 1200 to 2200 K, and the methyl recombination mechanism works

very well over this temperature range. Furthermore, optimized rate coefficients for R_2 from these experiments and dissociation of CH_3I[1] are in very good agreement.

Acknowledgment. This work was performed under the auspices of the Office of Basic Energy Sciences, Division of Chemical Sciences, Geosciences, and Biosciences, U.S. Department of Energy, under Contract Numbers DE-AC02-06CH11357, DE-AC04-94-AL85000, DE-FE-85ER13384.

Supporting Information Available: A table of the experimental conditions and k_1 and k_2 values is available. This information is available free of charge via the Internet at http://pubs.acs.org.

References and Notes

(1) Yang, X.; Goldsmith, C. F.; Tranter, R. S. *J. Phys Chem. A* DOI: jp903336u.
(2) Rice, F. O.; Walters, W. D. *J. Chem. Phys.* **1939**, *7* (11), 1015–1018.
(3) Walters, W. D. *J. Am. Chem. Soc.* **1940**, *62* (4), 880–886.
(4) Hole, K. J.; Mulcahy, M. F. R. *J. Phys. Chem.* **1969**, *73* (1), 177–185.
(5) Scherzer, K.; Plarre, D. *Z. Phys. Chem. (Leipzig)* **1975**, *256* (4), 660–672.
(6) Knoll, K. S.; Scherzer, K.; Geiseler, G. *Int. J. Chem. Kinet.* **1973**, *5* (2), 271–283.
(7) Guenther, W. B.; Whiteman, C. A.; Walters, W. D. *J. Am. Chem. Soc.* **1955**, *77* (8), 2191–2192.
(8) Blacet, F. E.; Bell, W. E. *Discuss. Faraday Soc.* **1954**, *14*, 70–76.
(9) Bell, W. E.; Blacet, F. E. *J. Am. Chem. Soc.* **1954**, *76* (21), 5332–5337.
(10) Frank, P.; Bhaskaran, K. A.; Just, T. *J. Phys. Chem.* **1986**, *90* (10), 2226–2231.
(11) Yasunaga, K.; Kubo, S.; Hoshikawa, H.; Kamesawa, T.; Hidaka, Y. *Int. J. Chem. Kinet.* **2008**, *40* (2), 73–102.
(12) Baulch, D. L.; Bowman, C. T.; Cobos, C. J.; Cox, R. A.; Just, T.; Kerr, J. A.; Pilling, M. J.; Stocker, D.; Troe, J.; Tsang, W.; Walker, R. W.; Warnatz, J. *J. Phys. Chem. Ref. Data* **2005**, *34* (3), 757–1397.
(13) Huynh, L. K.; Violi, A. *J. Org. Chem.* **2008**, *73* (1), 94–101.
(14) Senosiain, J. P.; Klippenstein, S. J.; Miller, J. A. *J. Phys. Chem. A* **2006**, *110* (17), 5772–5781.
(15) Lee, J.; Bozzelli, J. W. *Int. J. Chem. Kinet.* **2003**, *35* (1), 20–44.
(16) Tranter, R. S.; Giri, B. R. *Rev., Sci. Instrum.* **2008**, *79* (9), 094103.
(17) Kiefer, J. H.; Manson, A. C. *Rev. Sci. Instrum.* **1981**, *52* (9), 1392–1396.
(18) Kiefer, J. H., The Laser Schlieren Technique in Shock Tube Kinetics. In *Shock Waves in Chemistry*; Lifshitz, A., Ed.; Marcel Dekker: New York, 1981; pp 219−277.
(19) Gardiner, W. C.; Hidaka, Y.; Tanzawa, T. *Combust. Flame* **1981**, *40* (2), 213–219.
(20) Klippenstein, S. J. *J. Chem. Phys.* **1992**, *96* (1), 367–371.
(21) Klippenstein, S. J. *J. Phys. Chem.* **1994**, *98* (44), 11459–11464.
(22) Georgievskii, Y.; Klippenstein, S. J. *J. Chem. Phys.* **2003**, *118* (12), 5442–5455.
(23) Georgievskii, Y.; Klippenstein, S. J. VaReCoF; Sandia National Laboratories and Argonne National Laboratory, 2008.
(24) Miller, W. H. *J. Chem. Phys.* **1976**, *65* (6), 2216–2223.
(25) Klippenstein, S. J.; Khundkar, L. R.; Zewail, A. H.; Marcus, R. A. *J. Chem. Phys.* **1988**, *89* (8), 4761–4770.
(26) Dunning, T. H. *J. Chem. Phys.* **1989**, *90* (2), 1007–1023.
(27) Kendall, R. A.; Dunning, T. H.; Harrison, R. J. *J. Chem. Phys.* **1992**, *96* (9), 6796–6806.
(28) Klippenstein, S. J.; Georgievskii, Y.; Harding, L. B. *Phys. Chem. Chem. Phys.* **2006**, *8* (10), 1133–1147.
(29) Martin, J. M. L.; Uzan, O. *Chem. Phys. Lett.* **1998**, *282* (1), 16–24.
(30) *NIST Computational Chemistry Comparison and Benchmark Database*, NIST Standard Reference Database Number 101 Release 12, Aug 2005; Johnson, R. D., III, Ed.; http://srdata.nist.gov/cccbdb.
(31) Burcat, A.; Ruscic, B. *Ideal Gas Thermochemical Database with updates from Active Thermochemical Tables, March 2009*, ftp://ftp.technion.ac.il/pub/supported/aetdd/thermodynamics.
(32) Frisch, M. J.; Trucks, G. W.; Schlegel, H. B.; Scuseria, G. E.; Robb, M. A.; Cheeseman, J. R.; Montgomery, J. A., Jr.; Vreven, T.; Kudin, K. N.; Burant, J. C.; Millam, J. M.; Iyengar, S. S.; Tomasi, J.; Barone, V.; Mennucci, B.; Cossi, M.; Scalmani, G.; Rega, N.; Petersson, G. A.; Nakatsuji, H.; Hada, M.; Ehara, M.; Toyota, K.; Fukuda, R.; Hasegawa, J.; Ishida, M.; Nakajima, T.; Honda, Y.; Kitao, O.; Nakai, H.; Klene, M.; Li, X.; Knox, J. E.; Hratchian, H. P.; Cross, J. B.; Bakken, V.; Adamo, C.; Jaramillo, J.; Gomperts, R.; Stratmann, R. E.; Yazyev, O.; Austin, A. J.; Cammi, R.; Pomelli, C.; Ochterski, J. W.; Ayala, P. Y.; Morokuma, K.; Voth, G. A.; Salvador, P.; Dannenberg, J. J.; Zakrzewski, V. G.; Dapprich, S.; Daniels, A. D.; Strain, M. C.; Farkas, O.; Malick, D. K.; Rabuck, A. D.; Raghavachari, K.; Foresman, J. B.; Ortiz, J. V.; Cui, Q.; Baboul, A. G.; Clifford, S.; Cioslowski, J.; Stefanov, B. B.; Liu, G.; Liashenko, A.; Piskorz, P.; Komaromi, I.; Martin, R. L.; Fox, D. J.; Keith, T.; Al-Laham, M. A.; Peng, C. Y.; Nanayakkara, A.; Challacombe, M.; Gill, P. M. W.; Johnson, B.; Chen, W.; Wong, M. W.; Gonzalez, C.; Pople, J. A. *Gaussian 98, Revision A.7*; Gaussian, Inc.: Wallingford, CT, 2004.
(33) Werner, H.-J.; Knowles, P. J.; Lindh, R.; Manby, F. R.; Schütz, M.; Celani, P.; Korona, T.; Rauhut, G.; Amos, R. D.; Bernhardsson, A.; Berning, A.; Cooper, D. L.; Deegan, M. J. O.; Dobbyn, A. J.; Eckert, F.; Hampel, C.; Hetzer, G.; Lloyd, A. W.; McNicholas, S. J.; Meyer, W.; Mura, M. E.; Nicklass, A.; Palmieri, P.; Pitzer, R.; Schumann, U.; Stoll, H.; Stone A. J.; Tarroni, R., Thorsteinsson, T. *MOLPRO, Version 2006.1*.
(34) Lee, T. J.; Rendell, A. P.; Taylor, P. R. *J. Phys. Chem.* **1990**, *94* (14), 5463–5468.
(35) Harding, L. B.; Klippenstein, S. J.; Jasper, A. W. *Phys. Chem. Chem. Phys.* **2007**, *9* (31), 4055–4070.
(36) Miller, J. A.; Klippenstein, S. J. *J. Phys. Chem. A* **2006**, *110* (36), 10528–10544.
(37) Klippenstein, S. J.; Wagner, A. F.; Dunbar, R. C.; Wardlaw, D. M.; Robertson, S. H.; Miller, J. A. *Variflex, version 1.14m*; Argonne National Laboratory, 2006.
(38) Kiefer, J. H.; Alalami, M. Z.; Hajduk, J. C. *Appl. Opt.* **1981**, *20* (2), 221–230.
(39) Troe, J. *J. Chem. Phys.* **1977**, *66*, 4745–4757.
(40) Troe, J. *J. Chem. Phys.* **1977**, *66*, 4758–4775.
(41) Parkes, D. A. *Chem. Phys. Lett.* **1981**, *77* (3), 527–532.
(42) Timonen, R.; Kalliorinne, K.; Blomqvist, K.; Koskikallio, J. *Int. J. Chem. Kinet.* **1982**, *14* (1), 35–42.
(43) Anastasi, C.; Maw, P. R. *J. Chem. Soc., Faraday Trans. 1* **1982**, *78*, 2423–2433.
(44) Maricq, M. M.; Szente, J. J. *Chem. Phys. Lett.* **1996**, *253* (3−4), 333–339.
(45) Gardiner, W. C.; Walker B. F.; Wakefield C. B. , Mathematical Methods for Modelling Chemical Reactions. In *Shock Waves in Chemistry*; Lifshitz, A., Ed.; Marcel Dekker, Inc: New York, 1981; pp 319−374.
(46) Schliebs, R.; Knoll, H.; Scherzer, K. *React. Kinet. Catal. Lett.* **1976**, *5* (2), 141–147.
(47) Sato, K.; Hidaka, Y. *Combust. Flame* **2000**, *122* (3), 291–311.
(48) Kiefer, J. H.; Santhanam, S.; Srinivasan, N. K.; Tranter, R. S.; Klippenstein, S. J.; Oehlschlaeger, M. A. *Proc. Combust. Inst.* **2005**, *30*, 1129–1135.
(49) Woods, T.; Haynes, B. S. *Proc. Combust. Inst.* **1994**, *25*, 909–917.
(50) Adachi, H.; Basco, N.; James, D. G. L. *Int. J. Chem. Kinet.* **1981**, *13* (12), 1251–1276.

JP903716F